Lasers in Manufacturing Conference 2017

Numerical simulation of WC particles distribution in laser melt injection with external electromagnetic field support

Liang Wang[a,b], Jianhua Yao[a,b,*], Yong Hu[a,b], Qunli Zhang[a,b], Zhuo Sun[a,b], Rong Liu[c]

[a] *Institute of Laser Advanced Manufacturing, Zhejiang University of Technology, No.18 Chaowang Road, Hangzhou, 310014, China*
[b] *Zhejiang Provincial Collaborative Innovation Center of High-end Laser Manufacturing Equipment, Hangzhou, 310014, China*
[c] *Department of Mechanical and Aerospace Engineering, Carleton University, 1125 Colonel By Drive, Ottawa, Ontario, Canada K1S 5B6*

Abstract

An advanced particle distribution controlling approach is proposed for laser melt injection process, which applies an electric-magnetic compound field to assist the laser melt injection process. The electric-magnetic synergistic effect on the reinforcement particle distribution in laser melt injection is investigated using numerical and experimental methods. Spherical WC particles are used as the reinforcement and their distribution in the longitudinal sections of the laser melt injection layers is examined with SEM and studied with computer graphics processing. The distributions of fluid temperature, fluid velocity and reinforcement particles in the molten pool are simulated using a 2D multi-physics model coupled with the equations of heat transfer, fluid dynamics, drag force, Lorentz force and phase transition. The results show that, the directional Lorentz force due to an electric-magnetic compound field, as a sort of volume force, can change the equivalent buoyancy acting on the particles. When the Lorentz force and gravity force are in same direction, majority of particles are trapped in the upper region of laser melt injection layer, whereas most particles are concentrated in the bottom region. As a result, the distribution gradient of WC particles can be controlled by the electric-magnetic compound field, instead of the time-consuming adjustment of process parameters.

Keywords: Laser melt injection; Lorentz force; Distribution; Electric-magnetic compound field; Reinforcement particle;

* Corresponding author: Tel.: +86-571-88320383; Fax: +86-571-88320383-808.
E-mail address: laser@zjut.edu.cn.

1. Introduction

Metal matrix composites (MMCs) reinforced with ceramic particles display a number of advantages over monolithic alloys and have been used extensively in various industries such as automotive, aviation, aerospace and thermal management, etc.[1] . Laser melt injection (LMI) method is commonly employed to prepare a MMC layer on a metallic substrate, which exhibits special characteristics including low particle dissolution rate, high surface performance and low cracking tendency[2, 3]. Different from laser cladding process, the reinforcement particles (usually ceramics) that are injected in the molten pool without any other metalmatrix powders and move with the melt flow preserve solid state or micro melt state due to the rapid solidification in LMI process.

The graded distribution of reinforcement particles in metal matrix composites is a crucial optimization objective for LMI process, which can be designed at a microstructural level to tailor specific materials for their functional performance in particular applications[4]. For the efficient control of the distribution of WC particles, an external force is introduced during the LMI process, which applies an electric-magnetic compound field to the molten pool. A common coaxial nozzle can still be used to replace the special designed lateral nozzle thus to simplify the adjusting process of the powder delivery system.

The application of an electromagnetic field is a positive practice in laser welding and laser alloying to alter the distribution of added elements. The effect of electromagnetic stirring on the element distribution in laser welding was investigated in numerical and experimental methods. It was shown that the change of the distribution of the filler material resulted from a modulation of the melt flow due to the periodic induced electromagnetic volume forces. The frequency was a main parameter to determine the spatial distribution of elements, whereas the magnetic flux density was the main parameter determining the overall scale of the magnetic manipulation [5, 6]. A numerical model was built to investigate a laser molten aluminum pool under the influence of a steady magnetic field. The damped flow situation in the melt resulted in a variation of the solute distribution in the solid and in shallower alloyed layers, depending on the applied magnetic induction. The other effects of electromagnetic field included suppressing surface undulation of laser remelting [7], damping the velocity of molten pool[8, 9], reducing the defects of laser welding, preventing gravity dropout of the melt during laser full-penetration welding, etc. The previous investigations in electromagnetic field were mostly focused on the influences of elements, temperature, velocity and defect distribution on the molten pool during laser process, where an AC magnetic field or the melt flow in a steady magnetic field was present. Different from the solute distribution, the drag force and the buoyancy can highly influence the distribution of the reinforcement particles in the molten pool. The control effect of an electric-magnetic compound field on the distributions of fluid temperature, fluid velocity and reinforcement particles in the molten pool has not been investigated yet.

In the present research, a common coaxial nozzle is used with both an external steady electric field and a steady magnetic field applied in the molten pool synchronously during the LMI process. The Lorentz force is generated by the electric-magnetic synergistic effect, which is mainly a sort of directional volume force in the molten pool of LMI, similar to gravity. This Lorentz force can function as an additional volume force acting on the melt flow with variable direction. Consequently, the positions of WC particles trapped in the melting pool can be altered without changing LMI process parameters. A 2D transient multi-physics numerical model is employed to study the distribution mechanism of reinforcement particles during LMI under an electricmagnetic compound field. The partial differential equations, concerning Lorentz force, fluid dynamics, drag force acting on the particles, heat transfer and phase transition, are solved with COMSOL Multiphysics® 5.0. The simulation results are compared with experimental measurements and the influence of electric-magnetic compound field on the LMI process is discussed.

2. Experimental methods

AISI 316L austenitic stainless steel with dimensions of 200 × 20 × 10 mm was used as the substrate because of its paramagnetic property. The chemical composition of AISI 316L is listed in Table 1. Spherical WC particles were chosen as the reinforcement particles, because of good tracing performance in the melt flow. Accordingly, this shape was also used for the particles in the simulation study. The size of the WC particles was 75 ~ 150 μm. Fig. 1 illustrates the LMI process setup with an electric-magnetic compound field applied. The electromagnets were chosen to provide a steady magnetic field (max magnetic flux density of 2.0 T) and large capacity lead-acid batteries (2 V, 500 Ah) were used to provide high current (steady electric field) for the molten pool. The magnet poles with the size of 80 × 20 mm were applied in the experiment and numerical model. The specimen was placed in the center zone of the magnetic gap, where the distribution of magnetic flux density was uniform and the average current density was about 5 A/mm^2.

Table 1. Chemical composition (wt.%) of AISI316

C	Si	Mn	P	S	Ni	Cr	Mo	Fe
0.02	0.55	1.55	< 0.03	< 0.03	10.0	16.	2.08	Bal.

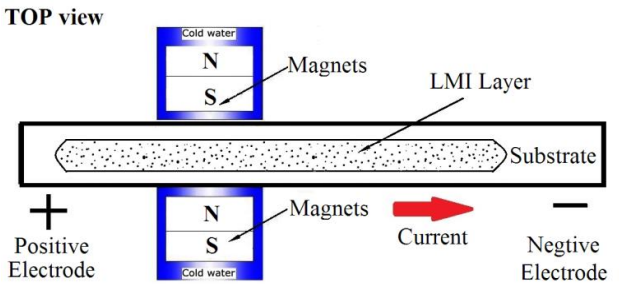

Fig. 1. Schematic diagram of LMI process setup with an electric-magnetic compound field

The LMI experiment was conducted using a 2 kW Laserline diode laser, self-made powder feeder and coaxial nozzle. Argon was used as the shielding gas to reduce oxidation of the specimen and WC particles. The laser beam diameter, optimal laser power, scanning speed and powder feeding ratio in this experiment were 4 mm, 1.7 kW, 4.25 mm/s and 15 g/min, respectively. The distributions of WC particles in the molten pool were examined using SEM (Carl Zeiss SIGMA HV-01-043).

3. Numerical simulation

3.1. Governing equations

During the LMI process, the particles are injected in the liquid molten pool, move with the melt flow and then be trapped in the solidification interface with the rapid cooling process of the molten pool. A classical computational fluid dynamics approach is applied to calculate the fluid flow field and pressure as well as the temperature of the molten pool. The movement of injected particles was computed using the Lagrangian approach with fluid–particle coupling [10]. The Lorentz force, as a sort of volume force, was included in the

source term of momentum equations. The 2D finite element model was composed of a rectangle of 30 × 5 mm. The necessary assumptions for the simulation model have been discussed in the reference[11].

The governing equations for mass conservation, energy conservation, momentum conservation, Darcy source, Lorentz force source and the movement of particles are solved using the finite element package COMSOL Multiphysics® 5.0. The detail discussion about the governing equations was listed in the reference [11].

The other required boundary conditions are illustrated together in Fig. 2.

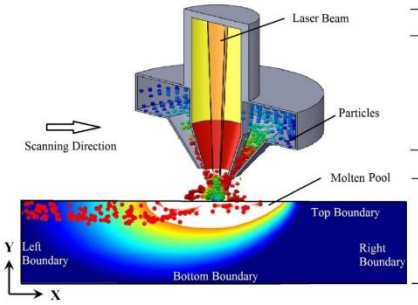

Velocity Boundary Condition	
Top Boundary	$-\eta u_{i,k} = \frac{\partial \gamma}{\partial T}\frac{\partial T}{\partial x_i}\ (i = 1, 2; k = 3)$
Left Boundary	$\mathbf{u} \cdot \mathbf{n} = 0$
Bottom Boundary	$\mathbf{u} \cdot \mathbf{n} = 0$
Right Boundary	$\mathbf{u} \cdot \mathbf{n} = 0$

Heat Boundary Condition	
Top Boundary	$q_0 = h \cdot (T_{ext} - T)$
Left Boundary	$q_0 = h \cdot (T_{ext} - T)$
Bottom Boundary	$-\mathbf{n} \cdot (-kVT) = 0$
Right Boundary	$q_0 = h \cdot (T_{ext} - T)$

Fig. 2. Boundary conditions of the numerical model

The physical properties of the molten pool and reinforcement particles are summarized in Table 3 [12-15]. The temperature-dependent properties of the AISI 316L steel are cited from the references [16-18].

Table 3. Material properties and parameters used in the simulation

Property	Symbol	Value	Unit
Melting point	T_m	1700	K
Fluid density	ρ	7850	kg·m
Dynamic viscosity	η	0.006	Pa·s
Thermal expansion coefficient	β	5×10^{-5}	K
Heat convection coefficient	h	20	W·m ·K
Surface tension coefficient	γ	1.76	N/m
Temperature derivative of the surface tension	$\partial\gamma / \partial T$	-5.2×10^{-4}	$N\cdot m^{-1}\cdot K^{-1}$
Particle density	ρ_p	15600	kg·m
Particle diameter	d_p	80	μm
Absorptivity	α	0.4	
Laser beam radius	r_l	2	mm

4. Numerical results

4.1. Velocity distribution

The velocity distribution in the longitudinal section of the molten pool is shown in Fig. 3. MN represents the direction of the directional Lorentz force. When MN = 1, the direction of Lorentz force is opposite to the gravity force. When MN = -1, the direction of Lorentz force coincides with the gravity force. The red arrows indicate the motion direction of fluid flow; the length of the arrows represents the magnitude of the motion

velocity of fluid flow and the green line represents the boundary of the molten pool. It is noted that the injected particles are removed in the figures for clearer appearance. The magnetic flux density is 0.8 T, the current density is 5 A/mm2, the laser power is 1.7 kW, the scanning speed is 4.25 mm/s and the powder feeding ratio is 15 g/min. Due to the Marangoni convection, the double vortices are observed in the molten pool and the fluid velocity in the near surface of the molten pool is much higher than that in the rest zone, as shown in Fig. 3(a). However, the global fluid velocity is reduced considerably in the molten pool with the electric-magnetic compound field applied, see Fig. 3(b) to (d). With the effect of an electric-magnetic field, there are two types of Lorentz force formed in the molten pool simultaneously, one is the directional Lorentz force and the other is the induced Lorentz force. The main reason for the observation in Fig. 3(b) is caused by the induced Lorentz force, which supports the suppression effect of the steady magnetic field [19-21]. Compared with the effect of the induced Lorentz force, the effect of the directional Lorentz force on the velocity distribution field is limited. In this case, the suppression effect of the magnetic field predominates the fluid velocity variation with the electric-magnetic compound field. As the directional Lorentz force induced by the electric-magnetic compound field is a sort of uniform volume force, which acts on the entire molten pool, it can alter the equivalent gravity force, but hardly accelerates or damps the fluid velocity.

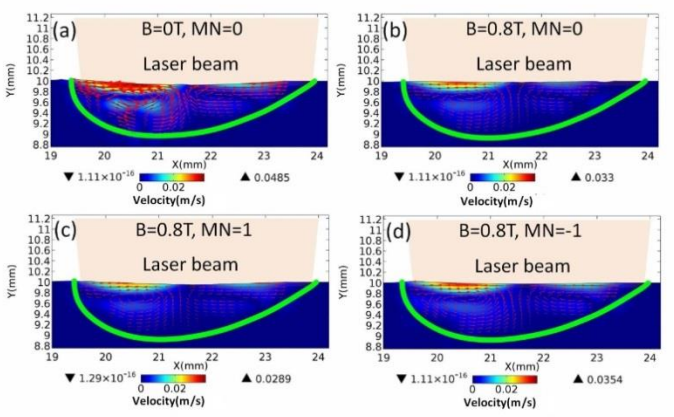

Fig. 3. Fluid velocity distribution in the molten pool at t = 3.9 s. (a) without magnetic field (B=0T, MN=0), (b) with only a steady magnetic field (B=0.8 T, MN=0), (c) with an electric-magnetic compound field (B=0.8 T, MN=1), (d) with an electric-magnetic compound field (B=0.8 T, MN=-1)

Hence, it is necessary to investigate the different effects between the induced Lorentz force due to fluid motion in a steady magnetic field and the directional Lorentz force induced by the electric-magnetic compound field. The surface fluid velocity of the molten pool with only a steady magnetic field is plotted in Fig. 4. The surface fluid velocity along the molten pool shows double-peak pattern. During the laser scanning process, on each side of the peak temperature location, thermal gradients are opposite in sign, which leads to the fluid flow velocity equal to zero at that point due to the Marangoni effect. The thermal gradients become maximal at the edge of the laser beam, which explains the velocity peaks observed [22]. With the increase of the magnetic flux density from 0 to 1.2 T, the maximum velocity at the surface of the molten pool is reduced from 0.048 to 0.024 m/s gradually, as shown in Fig. 4. When the magnetic flux density is up to 1.2 T, the peak velocity is only about half of that without the magnetic field applied. This is because the direction of the induced Lorentz force due to the steady magnetic field is always opposite to the direction of the fluid flow

defined by Eq. (6). These results confirm the strong damping effect of the steady magnetic field, which is consistent with the results of the literature[7, 8].

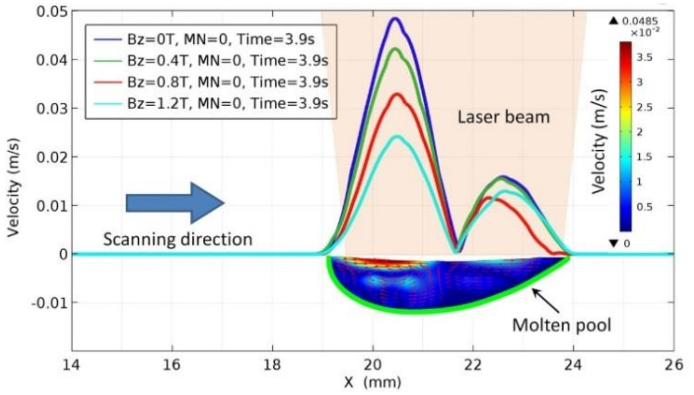

Fig. 4. Velocity distribution on the surface of molten pool in longitudinal direction with different magnetic flux densities

For further investigating the relationship between the velocity distribution and the directional Lorentz force, the surface fluid velocity of the molten pool with the electric-magnetic compound field present is plotted in Fig. 5. The magnetic flux density of the steady magnetic field is set to 0.8 T. The direction of the directional Lorentz force is kept unchanged and opposite to the gravity force. As illustrated in Fig. 5, whether the only steady magnetic field or the electric-magnetic compound field is applied, the fluid velocity at the surface of the molten pool decreases greatly due to the suppression effect of the steady magnetic field. However, under the condition of the electric-magnetic compound field applied, the maximum surface fluid velocity of the molten pool is changed slightly with the variation of the direction of the directional Lorentz force. When MN = -1, the maximum surface fluid velocity of the molten pool is higher than that in the cases of MN = 1 and MN = 0. When MN = 1, the maximum surface fluid velocity of the molten pool is even lower than that with the only steady magnetic field applied. Although the surface tension is the main driving force for the fluid motion of the molten pool [22], the natural convection is the secondary factor that can influence the fluid motion due to the nonuniformity of temperature distribution in the molten pool, which is expressed by the Boussinesq approximation . As a sort of volume force, when the directional Lorentz force is in the same direction with the gravity force, the equivalent gravity accelerant can be assumed to increase. The resultant natural convection is enhanced accordingly, which accelerates the fluid flow in a certain amount. When the direction of the directional Lorentz force is opposite to the gravity force, the effect of natural convection is reduced and the fluid velocity is then suppressed further. Combining the numerical results presented in Fig. 3 and Fig. 5, it is evident that the velocity distribution of the molten pool is related to the direction of the directional Lorentz force, but whose influence is less than that of the induced Loren force caused by the steady magnetic field.

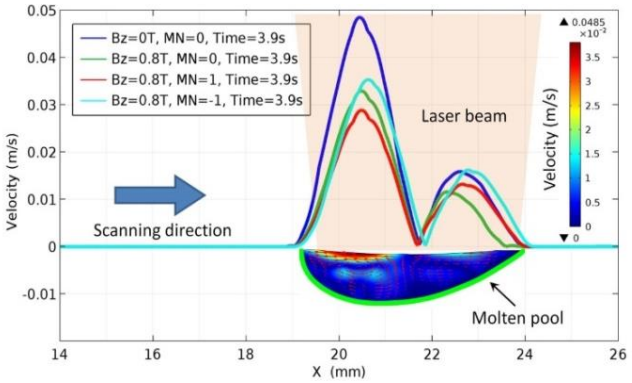

Fig. 5. Velocity distributions on the surface of molten pool in longitudinal direction with different directions of Lorenz force

4.2. Temperature distribution

The previous relevant investigation results had verified that the temperature distribution of molten pool was hardly changed under the effect a steady magnetic field during laser remelting process [7]. In order to compare the temperature distributions in the molten pool with and without the electric-magnetic compound field applied, the temperature distribution on the surface of the molten pool in longitudinal direction is plotted in Fig. 6. It is shown that when the single steady magnetic field or the electric-magnetic compound field is applied, the temperature in the surface center zone of the molten pool is only slightly higher than that without any external fields applied. The maximum rising range of the temperature is merely about 50K. The temperatures at the edge of the molten pool and in the unmelted zones are almost the same. The temperature distribution of the molten pool is little influenced by the direction of the directional Lorentz force. Different from the fluid velocity distribution, the temperature distribution is hardly influenced by the external field. It is inferred that with the present process parameters, the heat conduction predominates the temperature distribution of the molten pool, compared with the heat convection, which results in the change of fluid velocity insensitive to the temperature distribution of the motel pool.

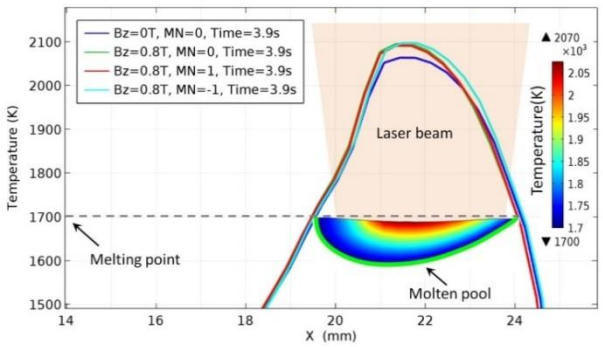

Fig. 6. Temperature distribution on the surface of molten pool in longitudinal direction with different directions of Lorenz force

In order to verify the above speculation, the Peclet number, as a dimensionless number, is introduced to show the ratio of the heat convection to the heat conduction. Fig. 7 illustrates the numerical results of Peclet

number distribution in the molten pool without any external fields. It is clear that the maximum Peclet number appears in the rear surface of the molten pool and the magnitude is only 0.824, where the maximum value of fluid velocity also occurs. In other zones of the molten pool, the Peclet number is far less than 1. Therefore, the heat conduction predominates the heat transfer of the molten pool there. It is foreseeable that with the addition of a steady magnetic field or electric-magnetic field, the Peclet number of molten pool and the effect of heat convection that is induced mainly by the fluid flow will all be reduced further. It can be inferred that the temperature distribution of the molten pool is mainly determined by the laser process parameters such as laser power, laser spot size and laser scanning velocity and so on. During the LMI process, solidification parameters such as the depth, the width and the solidification time of molten pool are almost the same under the conditions with and without the external magnetic or compound field. Meanwhile, the decomposing degree of the reinforcement particles in the LMI layer would nearly remain the same. This means that the original laser LMI parameters can be retained whether the electric-magnetic compound field is applied or not, which avoids the time-consuming adjustment.

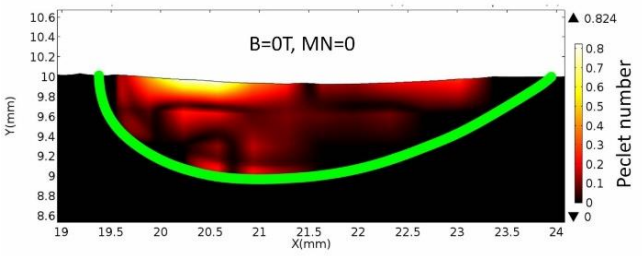

Fig. 7. Peclet number distribution of the molten pool

4.3. Particle distribution

The exact trapped positions of reinforcement particles are predicted by the simulation model in the condition that, magnetic flux density is 0.8 T, current density is 5 A/mm2, laser power is 1.7 kW, scanning speed is 4.25 mm/s and powder feeding rate is 15 g/min. The results are presented in Fig. 8, with the particle distributions for different directions of Lorentz force in the longitudinal sections of the LMI layers. The red dots represent the injected particles, the orientation of the tail indicates the motion direction of the particle and the length of the tail measures the magnitude of the motion velocity of the particle. With the same LMI process parameters, the number of injected particles, the depth of molten pool and the solidification time are all unchanged. Fig. 8 (c) shows that the particles are homogeneously distributed in the molten pool in the case without Lorentz force. This result indicates that the fluid flow in the molten pool is stirred adequately and the reinforcement particles can be trapped in the molten pool everywhere with the drag force of the melt flow under the present LMI process parameters condition.

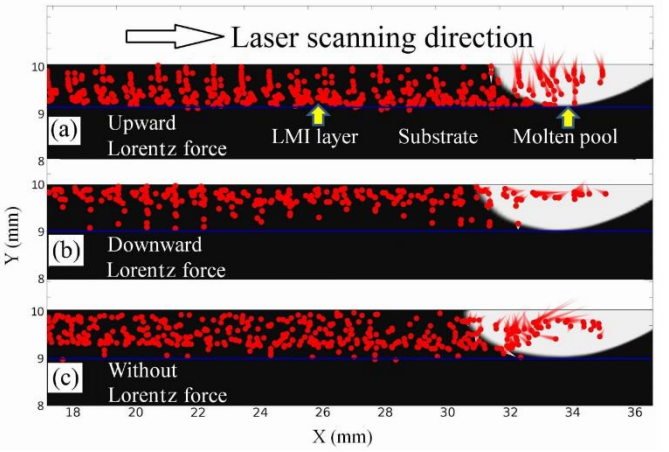

Fig. 8. Simulation results of WC particles distributions in longitudinal section of LMI layer. (a) Lorenz force upward, (b) Lorenz force downward, (c) Without Lorenz force

It is interesting to notice that with the presence of Lorentz force, the distributions of reinforcement particles are changed significantly. When the direction of Lorentz force is upward, most particles are concentrated in the lower region of the LMI layer, as shown in Fig. 8(a). This is because with the effect of electric-magnetic compound field, the fluid velocity in the near-surface zone (Marangoni convection zone) of the molten pool is damped greatly, as illustrated in Fig. 4. Meanwhile, the directional Lorentz force induced by the electric-magnetic compound field is a sort of volume force, similar to gravity force. When the direction of Lorentz force is opposite to gravity force, the equivalent gravity force acting on the fluid of molten pool is reduced. The resultant buoyancy acting on the particles is decreased accordingly. Hence, the sinking velocity of particles is increased. Therefore, when the particles are injected into the molten pool, the particles can quickly penetrate the Marangoni convection zone at the surface of molten pool and be easily sunk to the lower region of the molten pool before the solidification of the molten pool. With the effect of downward Lorentz force in the direction same to gravity force, the buoyancy acting on the particles is increased. The sinking velocity of the particles is reduced rapidly when they are injected into the molten pool. As a result, the particles can hardly penetrate the near surface zone, thus easier dragged to the edge of the molten pool even if the Marangoni convection in that zone is highly suppressed, where the molten pool is prone to solidify, as shown in Fig. 8(b). Consequently, most particles are trapped in the upper region of the molten pool. It is noted that the final trapped position of the particle is also related to the synchronously injecting position. The particles before injecting to the molten pool are assumed uniformly distributed on the surface of the molten pool in this model. In addition, the simulation results show that the effect of electric-magnetic compound field hardly influences the temperature distribution of the molten pool, which means that the solidification rate and the depth of the molten pool would remain unchanged. Therefore, under the same modeling boundary conditions during LMI process, the difference in overall distribution of the injected particles is certainly caused by the effect of directional Lorentz force.

5. Conclusion

The electric-magnetic synergistic effect on the reinforcement particle distribution in laser melt injection has been studied experimentally and numerically. Under the electric-magnetic compound field, both the induced Lorentz force and directional Lorentz force are formed in the molten pool. The induced Lorentz force produces the suppression effect on the velocity of the molten pool, which hardly influences the temperature distribution of the molten pool due to the small Peclet number, but the directional Lorentz force can change the equivalent buoyancy acting on the particles, which is the main factor controlling the distribution of reinforcement particles.

The distribution of reinforcement particles in the LMI layer can be easily tailored by the electric-magnetic compound field without adjusting LMI process parameters. When the Lorentz force and gravity force are in same direction, majority of particles are trapped in the upper region, while when the Lorentz force and gravity force are in opposite direction, most particles are concentrated in the lower region.

Acknowledgements

The authors are grateful for financial supports from the National Natural Science Foundation of China (51475429).

References

[1] D. Liu, Y. Chen, L. Li, F. Li, 2008. In situ investigation of fracture behavior in monocrystalline WCp-reinforced Ti–6Al–4V metal matrix composites produced by laser melt injection, Scripta Materialia 59, p. 91.

[2] Y.T. uPei, V. Ocelik, J.T.M., 2002. De Hosson, SiCp/Ti6Al4V functionally graded materials produced by laser melt injection, Acta Materialia 50, p. 2035.

[3] M. Cabeza, G. Castro, P. Merino, G. Pena, M. Roman, 2014. A study of laser melt injection of TiN particles to repair maraging tool steels, Surface and Interface Analysis 46, p. 861.

[4] J.A. Vreeling, V. Ocelík, J.T.M. De Hosson, 2002. Ti–6Al–4V strengthened by laser melt injection of WCp particles, Acta Materialia 50, p. 4913.

[5] Z. Tang, M. Gatzen, 2010. Influence on the dilution by laser welding of aluminum with magnetic stirring, Physics Procedia 5, p. 125.

[6] M. Gatzen, 2012. Influence of Low-frequency Magnetic Fields During Laser Beam Welding of Aluminium with Filler Wire, Physics Procedia 39, p. 59.

[7] L. Wang, J. Yao, Y. Hu, S. Song, 2015. Suppression effect of a steady magnetic field on molten pool during laser remelting, Applied Surface Science 351, p. 794.

[8] M. Bachmann, V. Avilov, A. Gumenyuk, M. Rethmeier, 2013. About the influence of a steady magnetic field on weld pool dynamics in partial penetration high power laser beam welding of thick aluminium parts, International Journal of Heat and Mass Transfer 60, p. 309.

[9] M. Bachmann, V. Avilov, A. Gumenyuk, M. Rethmeier, 2016. Numerical assessment and experimental verification of the influence of the Hartmann effect in laser beam welding processes by steady magnetic fields, International Journal of Thermal Sciences 101, p. 24.

[10] S. Yin, X. Wang, X. Suo, H. Liao, Z. Guo, W. Li, C. Coddet, 2013. Deposition behavior of thermally softened copper particles in cold spraying, Acta Materialia 61, p. 5105.

[11] L. Wang, J. Yao, Y. Hu, Q. Zhang, Z. Sun, R. Liu, 2017. Influence of electric-magnetic compound field on the WC particles distribution in laser melt injection, Surface and Coatings Technology 315, p. 32.

[12] T. Amine, J.W. Newkirk, F. Liou, 2014. Investigation of effect of process parameters on multilayer builds by direct metal deposition, Applied Thermal Engineering 73, p. 500.

[13] S.A. Khairallah, A. Anderson, 2014. Mesoscopic simulation model of selective laser melting of stainless steel powder, Journal of Materials Processing Technology 214, p. 2627.

[14] T. Heeling, K. Wegener, 2016. Computational Investigation of Synchronized Multibeam Strategies for the Selective Laser Melting Process, Physics Procedia 83, p. 899.
[15] S.Z. Shuja, B.S. Yilbas, H. Ali, C. Karatas, 2016. Laser pulse heating of steel mixing with WC particles in a irradiated region, Optics & Laser Technology 86, p. 126.
[16] J. Rahman Chukkan, M. Vasudevan, S. Muthukumaran, R. Ravi Kumar, N. Chandrasekhar, 2015. Simulation of laser butt welding of AISI 316L stainless steel sheet using various heat sources and experimental validation, Journal of Materials Processing Technology 219, p. 48.
[17] K.S. Kumar, 2015. Numerical Modeling and Simulation of a Butt Joint Welding Of AISI 316L Stainless Steels Using a Pulsed Laser Beam, Materials Today: Proceedings 2, p. 2256.
[18] T.K. Chu, C.Y. Ho, 1977. Thermal Conductivity and Electrical Resistivity of Eight Selected AISI Stainless Steels, Springer US.
[19] X. Cen, Y.S. Li, J. Zhan, 2012. Three dimensional simulation of melt flow in Czochralski crystal growth with steady magnetic fields, Journal of Crystal Growth 340, p. 135.
[20] O. Velde, R. Gritzki, R. Grundmann, 2001. Numerical investigations of Lorentz force influenced Marangoni convection relevant to aluminum surface alloying, International Journal of Heat and Mass Transfer, 44, p. 2751.
[21] B.H. Dennis, G.S. Dulikravich, 2002. Magnetic field suppression of melt flow in crystal growth, International Journal of Heat and Fluid Flow 23, p. 269.
[22] S. Morville, M. Carin, P. Peyre, M. Gharbi, D. Carron, P. Le Masson, R. Fabbro, 2012. 2D longitudinal modeling of heat transfer and fluid flow during multilayered direct laser metal deposition process, Journal of Laser Applications, 24.